

CFNS Summer School 2024: Intro to Small x Lecture Notes

Matthew D. Sievert

CHAPTER 1

L1: Origins of Small- x Evolution

1.1 Quark/Quark Scattering in Regge Kinematics

Scattering Amplitude

Consider the cross section for an elementary QCD process: elastic quark/quark scattering $q + q \rightarrow q + q$, as shown in Fig. 1.1. Let us work in the center-of-mass frame. In principle there are two diagrams: the t -channel amplitude (first diagram) and the u -channel amplitude (second diagram), which differ by a minus sign due to Fermi-Dirac statistics. Here we refer to the [Mandelstam variables](#)

$$s \equiv (p_1 + p_2)^2 = (p'_1 + p'_2)^2, \quad (1.1a)$$

$$t \equiv (p_1 - p'_1)^2 = (p'_2 - p_2)^2, \quad (1.1b)$$

$$u \equiv (p_1 - p'_2)^2 = (p_2 - p'_1)^2, \quad (1.1c)$$

$$s + t + u = 4m^2, \quad (1.1d)$$

which compactly describe the kinematics of a $2 \rightarrow 2$ process. A straightforward application of the Feynman rules from Appendix A in Feynman gauge yields:

$$i\mathcal{M} = i\mathcal{M}_t + i\mathcal{M}_u \quad (1.2a)$$

$$\begin{aligned} i\mathcal{M}_t &= [\bar{u}'_1 (ig\gamma_\mu (t^a)_{i'i}) u_1] \left(\frac{-ig^{\mu\nu} \delta^{ab}}{t} \right) [\bar{u}'_2 (ig\gamma_\nu (t^b)_{j'j}) u_2], \\ &= \frac{ig^2}{t} (t^a)_{i'i} (t^a)_{j'j} [\bar{u}'_1 \gamma_\mu u_1] [\bar{u}'_2 \gamma^\mu u_2] \end{aligned} \quad (1.2b)$$

$$\begin{aligned} i\mathcal{M}_u &= (-1)_{\text{Fermi}} [\bar{u}'_1 (ig\gamma_\mu (t^a)_{j'i}) u_2] \left(\frac{-ig^{\mu\nu} \delta^{ab}}{u} \right) [\bar{u}'_2 (ig\gamma_\nu (t^b)_{i'j}) u_1] \\ &= \frac{-ig^2}{u} (t^a)_{j'i} (t^a)_{i'j} [\bar{u}'_1 \gamma_\mu u_2] [\bar{u}'_2 \gamma^\mu u_1]. \end{aligned} \quad (1.2c)$$

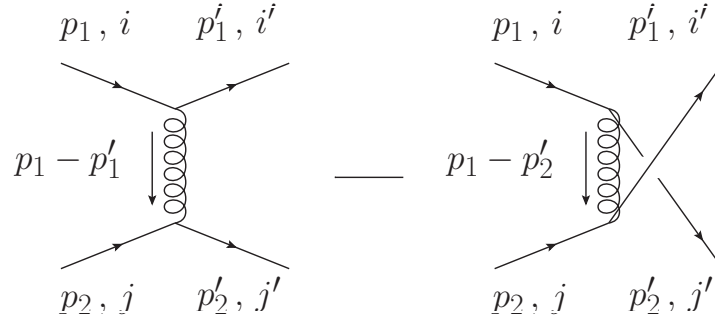


Figure 1.1: Quark-quark scattering amplitude to LO in QCD

High-Energy Kinematics: The Eikonal Approximation

Suppose we wish to study the behavior of the quark/quark scattering cross section in the **high-energy limit** $s \rightarrow \infty$. This is the limit relevant for high-energy collider experiments like the LHC, but we must take care to completely specify what we mean by this limit. When taking $s \rightarrow \infty$, we have two choices for what can happen to the other Mandelstam invariants. One possibility is that we increase the collision energy $s \rightarrow \infty$ and also the momentum transfer $|t| \rightarrow \infty$ proportionately. This is the **hard-scattering limit**, referred to as **Bjorken kinematics**, in which the scattering angle remains large at high energy because the exchanged momentum is growing large. In the language of deep inelastic scattering, this is the **large- x_B regime**. The other possibility is that we can take $s \rightarrow \infty$ while keeping $t = \text{const}$ fixed. This is the **forward-scattering limit**, known as **Regge kinematics**, in which the scattering angle decreases toward zero. In terms of DIS, this corresponds to the **small- x_B regime**.

Let us study the quark/quark cross section in Regge kinematics, for which

$$s \rightarrow \infty, \quad (1.3a)$$

$$t = \text{const}, \quad (1.3b)$$

$$u = 4m^2 - s - t \rightarrow -\infty. \quad (1.3c)$$

In this limit, the u -channel amplitude (which dominates for back-scattering, the opposite of Regge kinematics) is completely negligible, giving simply $i\mathcal{M} \approx i\mathcal{M}_t$. This is entirely natural, since the forward-scattering Regge regime is dominated by t -channel scattering.

In either Bjorken or Regge kinematics, it is very convenient to express the four-vectors in terms of **light-front components**, defined in Sec. A.3. Let us work in the center-of-mass frame with p_1^μ moving along the $-z$ axis and p_2^μ moving along the $+z$ axis. Then the relevant kinematics are

$$p_1^\mu \approx [0^+, p_1^-, \vec{0}_\perp], \quad (1.4a)$$

$$p_2^\mu \approx [p_2^+, 0^-, \vec{0}_\perp], \quad (1.4b)$$

1.1. Quark/Quark Scattering in Regge Kinematics

$$p_1'^{\mu} \approx \left[0^+, p_1'^-, \vec{p}'_{1\perp} \right], \quad (1.4c)$$

$$p_2'^{\mu} \approx \left[p_2'^+, 0^-, \vec{p}'_{2\perp} \right], \quad (1.4d)$$

with the Mandelstam invariants given by

$$s \approx 2p_2^+ p_1^-, \quad (1.5a)$$

$$t \approx -p_{1\perp}^2, \quad (1.5b)$$

$$u = 4m^2 - s - t \approx -s. \quad (1.5c)$$

In the strict center-of-mass frame, $p_1^- = p_2^+ = \sqrt{s/2}$.

In these high-energy kinematics, we have **approximate conservation of the separate momenta** p_1^-, p_2^+ :

$$p_1'^- \approx p_1^-, \quad (1.6a)$$

$$p_2'^+ \approx p_2^+, \quad (1.6b)$$

$$\vec{p}'_{1\perp} = -\vec{p}'_{2\perp}, \quad (1.6c)$$

with only a small transverse deflection $\vec{p}'_{1\perp}$ between them. This high-energy approximation, neglecting power-suppressed corrections in

$$\frac{1}{p_2^+} \sim \frac{1}{p_1^-} \sim \frac{1}{\sqrt{s}}, \quad (1.7)$$

is appropriate for Regge kinematics and is referred to as the **eikonal approximation**.

While we could compute the cross section by squaring the amplitude $i\mathcal{M} \approx i\mathcal{M}_t$, evaluating the traces, and then expanding the result in the eikonal limit $s \rightarrow \infty$, this becomes cumbersome at higher orders in perturbation theory. Instead, it is advantageous to directly simplify the amplitude itself to leading power in s . For the spinor products entering (1.2), this is most easily accomplished with the help of the [Gordon identity](#)

$$\bar{u}(p_1', s_1') \gamma^\mu u(p_1, s_1) = \bar{u}(p_1', s_1') \left[\frac{(p_1^\mu + p_1'^\mu)}{2m} + i\sigma^{\mu\nu} \frac{(p_1'_\nu - p_{1\nu})}{2m} \right] u(p_1, s_1) \quad (1.8)$$

with $\sigma^{\mu\nu} = \frac{i}{2}[\gamma^\mu, \gamma^\nu]$. To leading power in $p_1'^- = \sqrt{s/2}$, the incoming and outgoing momenta are equal:

$$p_1^\mu \approx p_1'^\mu \approx (\delta^\mu_-) p_1^-, \quad (1.9)$$

with corrections being suppressed by a relative factor of $\mathcal{O}(p_\perp/\sqrt{s})$. This allows us to neglect the second term of (1.8) in favor of the first term, which gives a

1. L1: Origins of Small- x Evolution

simple result for the spinor product:

$$\begin{aligned}
\bar{u}(p'_1, s'_1) \gamma^\mu u(p_1, s_1) &\approx \frac{(p'_1{}^\mu + p_1{}^\mu)}{2m} [\bar{u}(p'_1, s'_1) u(p_1, s_1)] \\
&\approx (\delta^\mu_-) \frac{p_1^-}{m} [\bar{u}(p_1^-, s'_1) u(p_1^-, s_1)] \\
&\approx 2 (\delta^\mu_-) p_1^- \delta_{s_1 s'_1} \\
&\approx 2 p_1^\mu \delta_{s_1 s'_1}, \tag{1.10}
\end{aligned}$$

neglecting relative corrections of order $\mathcal{O}(p_\perp/p_1^-)$. The same reasoning, applied to the other spinor product, yields

$$\bar{u}(p'_2, s'_2) \gamma^\mu u(p_2, s_2) \approx 2 p_2^\mu \delta_{s_2 s'_2}. \tag{1.11}$$

Together, this simplification to the t -channel amplitude gives

$$\begin{aligned}
i\mathcal{M} &\approx \frac{ig^2}{t} (t^a)_{i'i} (t^a)_{j'j} [\bar{u}'_1 \gamma_\mu u_1] [\bar{u}'_2 \gamma^\mu u_2] \\
&= \frac{4ig^2}{t} (t^a)_{i'i} (t^a)_{j'j} (p_1 \cdot p_2) \delta_{s_1 s'_1} \delta_{s_2 s'_2} \\
&= 2ig^2 \left(\frac{s}{t}\right) (t^a)_{i'i} (t^a)_{j'j} \delta_{s_1 s'_1} \delta_{s_2 s'_2}. \tag{1.12}
\end{aligned}$$

Cross Section

Only the t -channel amplitude contributes to the cross section at leading power in Regge kinematics, so the amplitude squared averaged over quantum numbers is given by

$$\begin{aligned}
\langle \mathcal{M}^2 \rangle &\equiv \frac{1}{4} \sum_{s_1 s'_1 s_2 s'_2} \frac{1}{N_c^2} \sum_{ii'jj'} (i\mathcal{M}_t) (i\mathcal{M}_t)^* \\
&= \frac{1}{4N_c^2} \sum_{s_1 s'_1 s_2 s'_2} \sum_{ii'jj'} \left((t^a)_{i'i} (t^a)_{j'j} (t^b)_{ii'} (t^b)_{jj'} \right) \left(4g^4 \frac{s^2}{t^2} \delta_{s_1 s'_1} \delta_{s_2 s'_2} \right) \\
&= \left(\frac{1}{N_c^2} \text{tr}[t^a t^b] \text{tr}[t^a t^b] \right) \left(4g^4 \frac{s^2}{t^2} \right). \tag{1.13}
\end{aligned}$$

The color traces can be evaluated for general N_c using the identities (A.5), giving the color factor

$$\frac{1}{N_c^2} \text{tr}[t^a t^b] \text{tr}[t^a t^b] = \frac{1}{2} \text{tr}[t^a t^a] = \frac{C_F}{2N_c^2} \text{tr}[\mathbf{1}] = \frac{C_F}{2N_c}. \tag{1.14}$$

The amplitude squared is then

$$\langle \mathcal{M}^2 \rangle = 4g^4 \left(\frac{C_F}{2N_c} \right) \frac{s^2}{t^2}. \tag{1.15}$$

1.1. Quark/Quark Scattering in Regge Kinematics

Given this expression for the amplitude squared, the corresponding differential cross section is

$$d\sigma = \frac{1}{2E_1 2E_2 |\vec{v}_1 - \vec{v}_2|} \frac{d^3 p'_1}{(2\pi)^3 2E'_1} \frac{d^3 p'_2}{(2\pi)^3 2E'_2} \langle \mathcal{M}^2 \rangle (2\pi)^4 \delta^4(p_1 + p_2 - p'_1 - p'_2). \quad (1.16)$$

In Regge kinematics, the flux prefactor is

$$\frac{1}{2E_1 2E_2 |\vec{v}_1 - \vec{v}_2|} = \frac{1}{8E_1 E_2} = \frac{1}{4p_1^- p_2^+} = \frac{1}{4p_1 \cdot p_2} = \frac{1}{2s}, \quad (1.17)$$

and we can change variables to light-front coordinates in the phase space and delta function, giving

$$d\sigma = \frac{1}{2s} \frac{d^2 p'_{1\perp} dp_1'^-}{2p_1'^-} \frac{d^2 p'_{2\perp} dp_2'^+}{2p_2'^+} \frac{\langle \mathcal{M}^2 \rangle}{(2\pi)^2} \delta(p_2^+ - p_2'^+) \delta(p_1^- - p_1'^-) \delta(\vec{p}'_{1\perp} + \vec{p}'_{2\perp}). \quad (1.18)$$

We can exhaust the constraints of the delta function by integrating over $p_1'^-$, $p_2'^+$, and \vec{p}'_2 to obtain

$$\begin{aligned} \frac{d\sigma}{d^2 p'_{1\perp}} &= \frac{1}{2s} \frac{1}{4p_1^- p_2^+} \frac{\langle \mathcal{M}^2 \rangle}{(2\pi)^2} \\ &= \frac{1}{(2s)^2} \frac{\langle \mathcal{M}^2 \rangle}{(2\pi)^2}. \end{aligned} \quad (1.19)$$

Finally, we insert the expression (1.15) for the amplitude squared, obtaining

$$\frac{d\sigma}{d^2 p'_{1\perp}} = 4\alpha_s^2 \frac{C_F}{2N_c} \frac{1}{p_{1\perp}'^4}. \quad (1.20)$$

in terms of $\alpha_s \equiv g^2/4\pi$ and using $t \approx -p_{1\perp}'^2$.

Integrating the differential cross section (1.20) over all $p'_{1\perp}$ yields the total (elastic) cross section at this order,

$$\begin{aligned} \sigma_{tot}|_{LO} &= 4\alpha_s^2 \frac{C_F}{2N_c} \int \frac{d^2 p'_{1\perp}}{p_{1\perp}'^4} \\ &= 4\pi\alpha_s^2 \frac{C_F}{2N_c} \int_{m^2}^{\infty} \frac{dp_{1\perp}^2}{p_{1\perp}'^4} \\ &= 4\pi\alpha_s^2 \frac{C_F}{2N_c} \frac{1}{m^2}. \end{aligned} \quad (1.21)$$

We note that the original integral $d^2 p'_{1\perp}/p_{1\perp}'^4$ has an infrared divergence as $p_{1\perp} \rightarrow 0$. This is an artifact of our use of bare quarks for the scattering; if we had instead used a color-neutral system (like a quark/antiquark dipole) then

1. L1: Origins of Small- x Evolution

the physical scale (the radius of the dipole) would cut this divergence off the in the IR. Since the exact numerical factors are unimportant for the present analysis, we just cut the $p_{1\perp}^2$ integral off with a scale of order the mass m in the infrared. For QCD with $N_c = 3$, we have $C_F = 4/3$ and $\frac{C_F}{2N_c} = \frac{2}{9}$.

The eikonal approximation (high-energy / small- x / Regge kinematics) has substantially simplified the cross section (1.20). Most importantly, the cross section for t -channel scattering at high energies is **unsuppressed as $s \rightarrow \infty$** . This is a general feature of high-energy scattering: the interactions are dominated by the exchange of vector bosons (such as gluons). Other processes mediated by the exchange of quarks (or even scalars in the case of scalar QCD) are suppressed by powers of s as $s \rightarrow \infty$, such that **eikonal scattering is always dominated by gluon exchange**. The gluons which mediate this high-energy scattering exchange no p_1^- or p_2^+ momenta between the high-energy quarks, essentially carrying only transverse momenta:

$$q^\mu \equiv (p_1 - p_1')^\mu \approx (0^+, 0^-, -\vec{p}'_{1\perp}). \quad (1.22)$$

These exchanged transverse gluons are referred to as **Glauber gluons** or **Coulomb gluons**, for which the only relevant dynamics is transverse to the eikonal collision axis.

1.2 Radiative Corrections: Soft QCD Bremsstrahlung

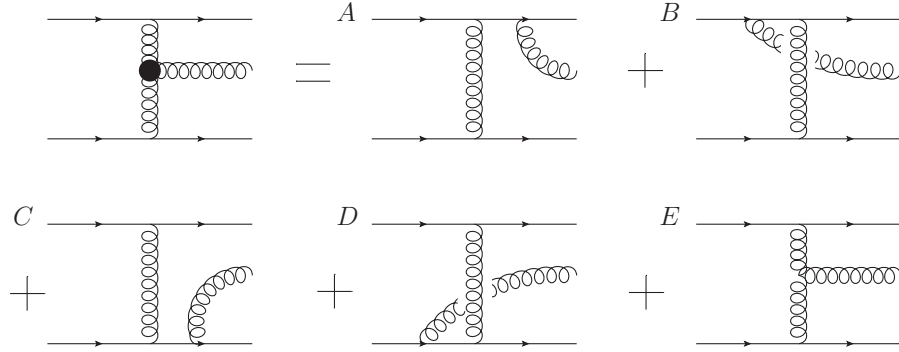


Figure 1.2: Feynman diagrams contributing to the scattering amplitude $i\mathcal{M}$ for the $2 \rightarrow 3$ radiative process $q + q \rightarrow q + q + g$. The sum of all the diagrams is represented by the thick effective vertex on the left, known as the **Lipatov vertex** (1.41).

Having computed the cross section for elastic $2 \rightarrow 2$ scattering of quarks ($q + q \rightarrow q + q$) in eikonal kinematics, let us next proceed to study **particle production** in this limit. The dominant mechanism of particle production in eikonal kinematics is the radiation of **soft gluon bremsstrahlung** as an NLO correction to the elastic scattering cross section we computed previously.

1.2. Radiative Corrections: Soft QCD Bremsstrahlung

The Feynman diagrams generating the leading contribution to $q+q \rightarrow q+q+g$ are shown in Fig. 1.2. There are 5 diagrams in total. Four of them (A-D) are totally analogous to the radiation of soft photons in QED; they consist of initial- and final-state radiation which can be emitted either from the “projectile” (p_1) or the “target” (p_2). The last diagram (E) is uniquely non-Abelian, in which the **exchanged gluon itself** undergoes bremsstrahlung.

As before, let us consider the case of eikonal scattering in Regge kinematics: $p_1^-, p_2^+ \sim \sqrt{s} \rightarrow \infty$. We will moreover focus on the case when the radiated gluon is “longitudinally soft,” meaning that its light-front momenta k^+, k^- are both small compared to the momenta of the incoming particles:

$$p_1^- \gg k^- \gg p_2^-, \quad (1.23a)$$

$$p_2^+ \gg k^+ \gg p_1^+. \quad (1.23b)$$

When expressed in terms of the **rapidity**

$$y = \frac{1}{2} \ln \frac{k^+}{k^-} \quad (1.24)$$

this means that we are looking at particle production at **mid-rapidity** $Y_2 \gg y \gg Y_1$. Particle production in this regime preserves the eikonal approximation because the radiated gluon does not disturb the flow of large p_1^- and p_2^+ through the diagram. This limit is also the limit in which the longitudinal momentum fraction called (Feynman) x is small, both with respect to the “projectile” p_1 and the “target” p_2 :

$$x_{F,proj} \equiv \frac{k^-}{p_1^-} \ll 1, \quad (1.25)$$

$$x_{F,tgt} \equiv \frac{k^+}{p_2^+} \ll 1. \quad (1.26)$$

Initial- vs. Final-State Radiation: Kinematics

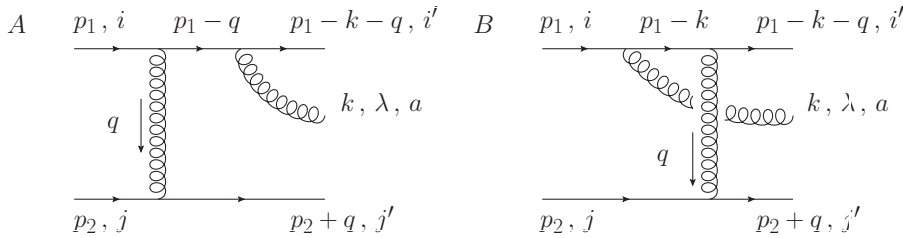


Figure 1.3: Initial-state (B) and final-state (A) radiation amplitudes for bremsstrahlung off the “projectile” p_1 .

Let us now compute in detail the final- and initial-state radiation diagrams A and B shown in Fig. 1.3. First let us specify the kinematics. For the incoming

1. L1: Origins of Small- x Evolution

particles we have the same kinematics as before:

$$p_1^\mu = \left[\frac{m^2}{2p_1^-}, p_1^-, \vec{0}_\perp \right]^\mu, \quad (1.27a)$$

$$p_2^\mu = \left[p_2^+, \frac{m^2}{2p_2^+}, \vec{0}_\perp \right]^\mu, \quad (1.27b)$$

while for the 3 final-state particles we have

$$\begin{aligned} (p_1 - k - q)^\mu &= \left[\frac{(\vec{k}_\perp + \vec{q}_\perp)^2 + m^2}{2(p_1^- - k^- - q^-)}, p_1^- - k^- - q^-, -\vec{k}_\perp - \vec{q}_\perp \right]^\mu \\ &\approx \left[\frac{(\vec{k}_\perp + \vec{q}_\perp)^2 + m^2}{2p_1^-}, p_1^-, -\vec{k}_\perp - \vec{q}_\perp \right]^\mu, \end{aligned} \quad (1.28a)$$

$$k^\mu = \left[k^+, \frac{k_\perp^2}{2k^+}, \vec{k}_\perp \right]^\mu, \quad (1.28b)$$

$$\begin{aligned} (p_2 + q)^\mu &= \left[p_2^+ + q^+, \frac{q_\perp^2 + m^2}{2(p_2^+ + q^+)}, \vec{q}_\perp \right]^\mu \\ &\approx \left[p_2^+, \frac{q_\perp^2 + m^2}{2p_2^+}, \vec{q}_\perp \right]^\mu. \end{aligned} \quad (1.28c)$$

This determines the exchanged momentum q^μ by momentum conservation:

$$\begin{aligned} q^\mu &= \left[q^+, q^-, \vec{q}_\perp \right]^\mu \\ &= \left[p_1^+ - k^+ - (p_1 - k - q)^+, (p_2 + q)^- - p_2^-, \vec{q}_\perp \right]^\mu \\ &\approx \left[-k^+, \frac{q_\perp^2}{2p_2^+}, \vec{q}_\perp \right]^\mu. \end{aligned} \quad (1.29)$$

Altogether, this gives for the eikonal limit $p_2^+ = p_1^- \rightarrow \infty$,

$$p_1^\mu \approx \left[0^+, p_1^-, \vec{0}_\perp \right]^\mu, \quad (1.30a)$$

$$p_2^\mu \approx \left[p_2^+, 0, \vec{0}_\perp \right]^\mu, \quad (1.30b)$$

$$k^\mu \approx \left[k^+, \frac{k_\perp^2}{2k^+}, \vec{k}_\perp \right]^\mu, \quad (1.30c)$$

$$q^\mu \approx \left[-k^+, \frac{q_\perp^2}{2p_2^+}, \vec{q}_\perp \right]^\mu, \quad (1.30d)$$

$$(p_1 - k - q)^\mu \approx \left[0^+, p_1^-, -\vec{k}_\perp - \vec{q}_\perp \right]^\mu, \quad (1.30e)$$

$$(p_2 + q)^\mu \approx \left[p_2^+, 0^-, \vec{q}_\perp \right]^\mu. \quad (1.30f)$$

1.2. Radiative Corrections: Soft QCD Bremsstrahlung

With the eikonal kinematics (1.30), it is straightforward to compute the virtualities of the intermediate-state particles for diagrams A and B. The exchanged gluon is the same for both diagrams:

$$\begin{aligned}
q^2 &= 2q^+q^- - q_\perp^2 \\
&= -\frac{k^+}{p_2^+}q_\perp^2 - q_\perp^2 \\
&\approx -q_\perp^2,
\end{aligned} \tag{1.31}$$

just as with the elastic scattering process we computed before. The intermediate quark propagators are different for the two diagrams, giving

$$\begin{aligned}
(p_1 - q)^2 &= 2(p_1^+ - q^+)(p_1^- - q^-) - (\vec{p}_{1\perp} - \vec{q}_\perp)^2 \\
&\approx 2(0^+ + k^+)(p_1^- - \frac{q_\perp^2}{2p_2^+}) - q_\perp^2 \\
(p_1 - q)^2 &\approx 2k^+p_1^-,
\end{aligned} \tag{1.32a}$$

$$\begin{aligned}
(p_1 - k)^2 &= 2(p_1^+ - k^+)(p_1^- - k^-) - (\vec{p}_{1\perp} - \vec{k}_\perp)^2 \\
&\approx 2(0^+ - k^+)(p_1^- - \frac{k_\perp^2}{2k^+}) - q_\perp^2 \\
&\approx -2k^+p_1^-.
\end{aligned} \tag{1.32b}$$

Crucially, the virtualities of these two intermediate states are **exactly opposite** in the high-energy limit, and this virtuality is small compared to the collision energy s :

$$(p_1 - q)^2 \approx -(p_1 - k)^2 \approx 2k^+p_1^- \ll s. \tag{1.33}$$

This shows that the **kinematics of the two diagrams are identical, but different by a sign** accounting for the fact that the propagator is timelike for diagram A but spacelike for diagram B.

Initial- vs. Final-State Radiation: Amplitudes

The evaluation of the amplitudes for diagrams A and B is now straightforward. For diagram A in Feynman gauge we have

$$\begin{aligned}
i\mathcal{M}_A &= [\bar{u}'_1 (ig\not{\epsilon}_\lambda^*(t^a)_{i'i''}) \left(\frac{i(\not{p}_1 - \not{q})}{(p_1 - q)^2} \right) (ig\gamma_\mu(t^b)_{i''i}) u_1] \\
&\quad \times \left(\frac{-ig^{\mu\nu}\delta^{bb'}}{q^2} \right) [\bar{u}'_2 (ig\gamma_\nu(t^{b'})_{j'j}) u_2] \\
&= \frac{+ig^3}{q_\perp^2 (2k^+p_1^-)} (t^a t^b)_{i'i} (t^b)_{j'j} [\bar{u}'_1 \not{\epsilon}_\lambda^*(\not{p}_1 - \not{q}) \gamma_\mu u_1] [\bar{u}'_2 \gamma^\mu u_2].
\end{aligned} \tag{1.34}$$

1. L1: Origins of Small- x Evolution

Again utilizing the Gordon identity (1.8) in the eikonal limit, we write the spinor product for the target as

$$[\bar{u}'_2 \gamma^\mu u_2] \approx 2p_2^+ \delta^\mu_+ \delta_{s_2 s'_2}. \quad (1.35)$$

This sets $\mu = +$ in the spinor matrix element for the projectile (recall that $\gamma_+ = \gamma^-$), and we can further eikonalize the spinor matrix element:

$$\begin{aligned} [\bar{u}'_1 \not{\epsilon}_\lambda^* (\not{p}_1 - \not{q}) \gamma^- u_1] &\approx p_1^- [\bar{u}'_1 \not{\epsilon}_\lambda^* \gamma^+ \gamma^- u_1] \\ &= p_1^- [\bar{u}'_1 \not{\epsilon}_\lambda^* \{\gamma^+, \gamma^-\} u_1] \\ &= 2p_1^- [\bar{u}'_1 \not{\epsilon}_\lambda^* u_1] \\ &= 2p_1^- (\epsilon_\lambda^*)_\mu [\bar{u}'_1 \gamma^\mu u_1] \\ &\approx 2p_1^- (\epsilon_\lambda^*)_\mu (2p_1^- \delta^\mu_+ - \delta_{s_1 s'_1}) \\ &= (2p_1^-)^2 (\epsilon_\lambda^*)^+ \delta_{s_1 s'_1} \end{aligned} \quad (1.36)$$

where we have used the Dirac equation

$$\begin{aligned} (\not{p}_1 - m) u_1 &\approx p_1^- \gamma^+ u_1 = 0 \\ \therefore \gamma^+ u_1 &= 0 \end{aligned} \quad (1.37)$$

for the incoming quark at eikonal accuracy. Substituting these results back into (1.34) gives

$$\begin{aligned} i\mathcal{M}_A &= \frac{+ig^3}{q_\perp^2 (2k^+ p_1^-)} (t^a t^b)_{i'i} (t^b)_{j'j} (2p_2^+ \delta_{s_2 s'_2}) ((2p_1^-)^2 (\epsilon_\lambda^*)^+ \delta_{s_1 s'_1}) \\ &= ig^3 \frac{2s (\epsilon_\lambda^*)^+}{q_\perp^2 k^+} (t^a t^b)_{i'i} (t^b)_{j'j} \delta_{s_1 s'_1} \delta_{s_2 s'_2}. \end{aligned} \quad (1.38)$$

In a similar way, we can evaluate amplitude B in the eikonal approximation:

$$\begin{aligned} i\mathcal{M}_B &= [\bar{u}'_1 (ig\gamma_\mu (t^b)_{i'i'}) \left(\frac{i(\not{p}_1 - \not{k})}{(p_1 - k)^2} \right) (ig\not{\epsilon}_\lambda^* (t^a)_{i''i}) u_1] \\ &\quad \times \left(\frac{-ig^{\mu\nu} \delta^{bb'}}{q^2} \right) [\bar{u}'_2 (ig\gamma_\nu (t^{b'})_{j'j}) u_2] \\ &= \frac{+ig^3}{q_\perp^2 (-2k^+ p_1^-)} (t^b t^a)_{i'i} (t^b)_{j'j} [\bar{u}'_1 \gamma_\mu (\not{p}_1 - \not{k}) \not{\epsilon}_\lambda^* u_1] [\bar{u}'_2 \gamma^\mu u_2] \\ &= \frac{+ig^3}{q_\perp^2 (-2k^+ p_1^-)} (t^b t^a)_{i'i} (t^b)_{j'j} [\bar{u}'_1 \gamma^- (\not{p}_1 - \not{k}) \not{\epsilon}_\lambda^* u_1] (2p_2^+ \delta_{s_2 s'_2}) \end{aligned}$$

1.2. Radiative Corrections: Soft QCD Bremsstrahlung

$$\begin{aligned}
&= -ig^3 \frac{2p_1^- p_2^+}{q_\perp^2} \frac{1}{2k^+ p_1^-} (t^b t^a)_{i' i} (t^b)_{j' j} \delta_{s_2 s_2'} [\bar{u}'_1 \gamma^- \gamma^+ \not{\epsilon}_\lambda^* u_1] \\
&= -ig^3 \frac{2s}{q_\perp^2} \frac{1}{2k^+ p_1^-} (t^b t^a)_{i' i} (t^b)_{j' j} \delta_{s_2 s_2'} [\bar{u}'_1 \not{\epsilon}_\lambda^* u_1] \\
i\mathcal{M}_B &= -ig^3 \frac{2s}{q_\perp^2} \frac{(\epsilon_\lambda^*)^+}{k^+} (t^b t^a)_{i' i} (t^b)_{j' j} \delta_{s_1 s_1'} \delta_{s_2 s_2'}. \tag{1.39}
\end{aligned}$$

Discussion

Comparing the final-state radiation diagram $i\mathcal{M}_A$ from Eq. (1.38) with the initial-state radiation diagram $i\mathcal{M}_B$, from Eq. (1.39), we make several interesting observations:

- These two amplitudes are **almost identical**, owing to the eikonal kinematics of the Regge scattering. The dependence on all kinematic variables is the same.
- The amplitudes are proportional to $1/k^+$, and since $k^+ \ll p_2^+$ is a soft momentum scale, the amplitude to radiate a soft gluon is **parametrically large**.
- The eikonal limit is in general **spin-independent**. This means we must work harder and include **sub-eikonal corrections** if we want to describe the behavior of **spin asymmetries** in Regge kinematics.
- The two amplitudes differ by a minus sign. This sign difference came from Eq. (1.33), arising because the **only** kinematic difference between the two amplitudes is that for diagram A, the propagator is timelike (k^+ and p_1^- flowing in the same direction), while for diagram B, it is spacelike (k^+ and p_1^- flowing in opposite directions).
- Aside from the minus sign, the only other difference between the two amplitudes is the **order of the two color rotations** of the projectile quark. For diagram A, the scattering occurs before the radiation, leading to the combined color rotation $(t^a t^b)_{i' i}$. For diagram B, the radiation vertex occurs first, leading to $(t^b t^a)_{i' i}$.
- In the eikonal approximation, both amplitudes to radiate the gluon from the projectile are proportional to the polarization vector $(\epsilon_\lambda^*)^+$. This means that if we strategically **choose a gauge** such that $(\epsilon_\lambda^*)^+ = 0$ (the light-front gauge $A^+ = 0$), then $i\mathcal{M}_A = i\mathcal{M}_B = 0$. This allows us to **suppress radiation from the projectile in this special gauge**, leaving only contributions from the other diagrams C, D, E. The same is true for the target: choosing the light-front gauge $A^- = 0$ suppresses

1. L1: Origins of Small- x Evolution

radiation from the target, resulting in $i\mathcal{M}_C = i\mathcal{M}_D = 0$. An appropriate choice of gauge like this can drastically simplify the calculation.

- In a symmetric gauge like Feynman gauge, diagrams C and D, being mirror images of A and B, can be trivially obtained from Eqs. (1.38) and (1.39) by appropriate **substitution of the momenta**.

Understanding the general form of the bremsstrahlung amplitude in eikonal kinematics leads to a profound difference between the radiation pattern produced by QED and by QCD. Adding the two amplitudes together, we obtain

$$\begin{aligned}
 i\mathcal{M}_A + i\mathcal{M}_B &= ig^3 \frac{2s}{q_\perp^2} \frac{(\epsilon_\lambda^*)^+}{k^+} ((t^a t^b)_{i'i} - (t^b t^a)_{i'i}) (t^b)_{j'j} \delta_{s_1 s'_1} \delta_{s_2 s'_2} \\
 &= ig^3 \frac{2s}{q_\perp^2} \frac{(\epsilon_\lambda^*)^+}{k^+} [t^a, t^b]_{i'i} (t^b)_{j'j} \delta_{s_1 s'_1} \delta_{s_2 s'_2} \\
 &= ig^3 \frac{2s}{q_\perp^2} \frac{(\epsilon_\lambda^*)^+}{k^+} (i f^{abc} (t^c)_{i'i}) (t^b)_{j'j} \delta_{s_1 s'_1} \delta_{s_2 s'_2} \\
 &= -g^3 f^{abc} (t^c)_{i'i} (t^b)_{j'j} \frac{2s}{q_\perp^2} \frac{(\epsilon_\lambda^*)^+}{k^+} \delta_{s_1 s'_1} \delta_{s_2 s'_2} . \tag{1.40}
 \end{aligned}$$

The relative minus sign between the initial-state- and final-state-radiation diagrams, together with the reversed order of the color rotations, has produced a **commutator** of the color matrices. This changes the combined color structure to something proportional to the structure constants f^{abc} – exactly of the same form as diagram E containing the triple-gluon vertex. Thus all of the diagrams A-E can be combined into a single structure with an effective 3-gluon vertex, known as the **Lipatov vertex**, as depicted in Fig. 1.2.

The difference here between QED and QCD could not be more pronounced. In QCD, the initial-state radiation diagrams combine with the final-state radiation diagrams in a systematic way, leading to parametrically large rate of particle production at high energies. But in QED, without the presence of the non-Abelian $SU(N_c)$ generators, the **amplitudes simply cancel instead**, and diagram E does not exist. For electron/electron scattering in QED at high energies, **no net photon radiation is produced**, and the Regge limit is trivial and uninteresting. This just corresponds to the familiar semi-classical statement that an electron must **accelerate** to produce radiation, and since $s \rightarrow \infty$ with t fixed, the scattering angle goes to zero and the electrons do not accelerate. But in QCD, the quarks have an internal color degree of freedom as well as their kinematic variables. Unlike electrons, quarks can “accelerate” in color space, leading to a proliferation of soft gluon radiation at mid rapidity. Thus the high-energy Regge limit (small x_F) is **uniquely sensitive to the non-Abelian nature of QCD**. And, moreover, **any non-Abelian gauge theory** (not just QCD) will produce an abundance of soft gluon radiation – directly as a consequence of the non-commutative vertex.

Cross Section and Gluon Multiplicity

A complete calculation of all the diagrams in Fig. 1.2 leads to the full amplitude

$$i\mathcal{M} = -g^3 f^{abc} (t^c)_{i'i} (t^b)_{j'j} \frac{4s}{q_\perp^2} (\epsilon_\lambda^*)_\mu \left(\frac{k_\perp^\mu}{k_\perp^2} - \frac{(k+q)_\perp^\mu}{(k+q)_\perp^2} \right) \delta_{s_1 s'_1} \delta_{s_2 s'_2}. \quad (1.41)$$

As promised, this diagram has the color structure of the 3-gluon vertex, along with a characteristic transverse momentum dependence which defines the Lipatov vertex. Squaring the amplitude and summing/averaging over the spin and color quantum numbers yields

$$\langle |\mathcal{M}|^2 \rangle = 8g^3 C_F \frac{s^2}{q_\perp^2 k_\perp^2 (k+q)_\perp^2} \quad (1.42)$$

and to the differential cross section

$$\frac{d\sigma}{d^2 k_\perp d^2 q_\perp dy} = \frac{2\alpha_s^3 C_F}{\pi^2} \frac{1}{q_\perp^2 k_\perp^2 (k+q)_\perp^2}. \quad (1.43)$$

For the cross section differential only in the kinematics of the produced gluon, we integrate over $d^2 q_\perp$:

$$\begin{aligned} \frac{d\sigma}{d^2 k_\perp dy} &= \frac{2\alpha_s^3 C_F}{\pi^2} \frac{1}{k_\perp^2} \int \frac{d^2 q_\perp}{q_\perp^2 (k+q)_\perp^2} \\ &= \frac{2\alpha_s^3 C_F}{\pi^2} \frac{1}{k_\perp^2} \int_0^1 d\alpha \int \frac{d^2 q_\perp}{\left[(\vec{q}_\perp + (1-\alpha)\vec{k}_\perp)^2 + \alpha(1-\alpha)k_\perp^2 + m^2 \right]^2} \\ &= \frac{2\alpha_s^3 C_F}{\pi^2} \frac{1}{k_\perp^2} \int_0^1 d\alpha \frac{\pi}{\alpha(1-\alpha)k_\perp^2 + m^2} \\ &\approx \frac{4\alpha_s^3 C_F}{\pi} \frac{m^2}{k_\perp^4} \ln \frac{k_\perp^2}{m^2}, \end{aligned} \quad (1.44)$$

where we computed the integral using Feynman parameters and regulated the IR divergence by adding a mass m^2 as a regulator $m^2 \rightarrow 0$.

The cross section $\frac{d\sigma}{d^2 k_\perp dy}$ describes the distribution of produced gluons as a function of their kinematics k^μ , but it is difficult to interpret because the numerator $d\sigma$ has units of area. We can define a more natural **gluon multiplicity** by normalizing the differential cross section $\frac{d\sigma}{d^2 k_\perp dy}$ by the elastic scattering cross section (1.21):

$$\frac{dN^g}{d^2 k_\perp dy} \equiv \frac{1}{\sigma_{el}} \frac{d\sigma}{d^2 k_\perp dy} = \frac{2\alpha_s N_c}{\pi^2} \frac{m^4}{k_\perp^4} \ln \frac{k_\perp^2}{m^2}. \quad (1.45)$$

1. L1: Origins of Small- x Evolution

Integrating the gluon multiplicity over d^2k_\perp gives the multiplicity per unit rapidity,

$$\begin{aligned} \frac{dN^g}{dy} &\equiv \int d^2k_\perp \frac{dN^g}{d^2k_\perp dy} \\ &= \frac{2\alpha_s N_c}{\pi^2} \int_{m^2}^{\infty} d^2k_\perp \frac{m^4}{k_\perp^4} \ln \frac{k_\perp^2}{m^2} \\ &\approx \frac{2\alpha_s N_c}{\pi^2}, \end{aligned} \quad (1.46)$$

where we again cut off the k_\perp integral with a mass at the lower end to regulate the IR divergence. One final integral over the rapidity y yields the total expected number of gluons emitted:

$$N_{tot}^g \equiv \int_{Y_1}^{Y_2} dy \frac{dN^g}{dy} = \frac{2\alpha_s N_c}{\pi^2} (Y_2 - Y_1). \quad (1.47)$$

The total rapidity interval $\Delta Y = Y_2 - Y_1$ covered by the collision is determined by the center-of-mass energy s available. Combining the incident-particle kinematics (1.27) with the definition (1.24) of rapidity, we can write the rapidity interval as a logarithm of s :

$$\begin{aligned} Y_2 - Y_1 &= \frac{1}{2} \ln \frac{p_2^+}{p_2^-} - \frac{1}{2} \ln \frac{p_1^+}{p_1^-} \\ &= \frac{1}{2} \ln \frac{p_1^- p_2^+}{p_1^+ p_2^-} \\ &= \frac{1}{2} \ln \frac{(s/2)}{(m^4/2s)} \\ &= \ln \frac{s}{m^2}. \end{aligned} \quad (1.48)$$

Then the **total expected number of gluons grows as a logarithm of the center-of-mass energy s :**

$$N_{tot}^g = \frac{2\alpha_s N_c}{\pi^2} \ln \frac{s}{m^2}. \quad (1.49)$$

Discussion

Here, we have computed both the elastic scattering $qq \rightarrow qq$ and gluon production $qq \rightarrow qgq$ cross sections in the high-energy Regge limit. Summarizing the results, we found that

$$\sigma_{el} = 4\pi\alpha_s^2 \frac{C_F}{2N_c} \frac{1}{m^2}, \quad (1.50a)$$

1.2. Radiative Corrections: Soft QCD Bremsstrahlung

$$\frac{d\sigma}{d^2k_\perp dy} = \frac{4\alpha_s^3 C_F m^2}{\pi k_\perp^4} \ln \frac{k_\perp^2}{m^2}, \quad (1.50b)$$

$$\frac{dN^g}{d^2k_\perp dy} = \frac{2\alpha_s N_c}{\pi^2} \frac{m^4}{k_\perp^4} \ln \frac{k_\perp^2}{m^2}, \quad (1.50c)$$

$$\frac{dN^g}{dy} = \frac{2\alpha_s N_c}{\pi^2}, \quad (1.50d)$$

$$N_{tot}^g = \frac{2\alpha_s N_c}{\pi^2} \ln \frac{s}{m^2}. \quad (1.50e)$$

These results were computed to eikonal accuracy in the kinematics, and using a mass scale m^2 in various places to cut off the IR divergences associated with our choice of free quarks as the projectile / target.

Some features of these results are specific to the simple quark model being computed. For instance, in this calculation, the transverse momentum dependence of the gluon multiplicity is a pure $1/k_\perp^4$ power law (up to a slowly-varying logarithm). This is characteristic of a pointlike source of gluons (the colliding quarks) and will be modified if the projectile / target are replaced with an extended object (for instance, a quark/antiquark dipole). But the **rapidity (in)dependence** of the gluon multiplicity $dN^g/d^2k_\perp dy$ section is quite generic, following simply from the eikonal approximation and the form of the quark/gluon vertex in QCD. In fact, we would have found the same scaling,

$$\frac{dN^g}{dy} \sim \alpha_s \times (\text{const}) \quad , \quad N^g \sim \alpha_s \times \ln \frac{s}{m^2} \times (\text{const})$$

if we had considered the eikonal scattering of *gluons* instead of quarks.

A robust prediction of QCD for any high-energy hadronic scattering process is **the emission of a spectrum of soft gluon radiation which is uniform (boost-invariant) at mid-rapidity**. This is exactly what is seen experimentally from particle production (here: inclusive charged hadrons) at mid-rapidity in high-energy hadronic collisions (Fig. 1.4). We find that **QCD produces an abundance of soft gluon radiation at high energies** which is **boost-invariant** (rapidity-independent) at leading power in the eikonal expansion.

Even more profoundly, that constancy of the gluon spectrum with rapidity sets up a dynamic **competition** between the parametrically **small probability** to emit a gluon in perturbative QCD ($\alpha_s \ll 1$) and the **large phase space** of rapidity available to the gluon ($\Delta Y = \ln s/m^2 \gg 1$). The expected number of gluons is nominally computed in weak-coupling perturbation theory

$$N^g \sim \alpha_s \times \ln \frac{s}{m^2} \times (\text{const}) + \mathcal{O}(\alpha_s^2) \quad (1.51)$$

as an $\mathcal{O}(\alpha_s)$ NLO correction relative to the elastic scattering. As such, is a parametrically small quantity: $N_g \sim \alpha_s \ll 1$ as long as the logarithm is of order unity.

But when s is **very** large – not just “kinematically large”, $s \gg m^2$, but **exponentially large**, $\ln \frac{s}{m^2} \gg 1$ – the dimensionless logarithm begins to

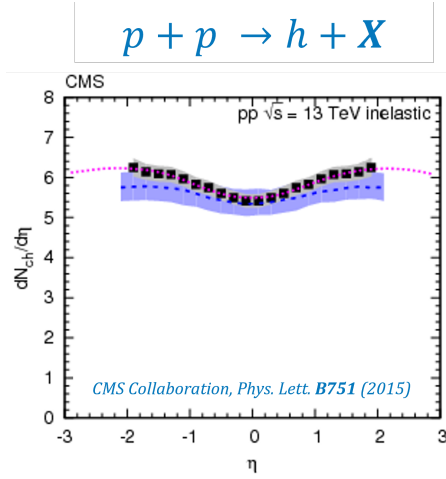


Figure 1.4: A uniform distribution of hadrons at mid-rapidity measured by the CMS Collaboration, in excellent agreement with our expectations from the tree-level calculation in QCD.

compete with the expansion parameter α_s of perturbation theory. When the phase space is large enough to fully offset the the suppression in the coupling,

$$\alpha_s \ln \frac{s}{m^2} \sim \mathcal{O}(1) \quad \leftrightarrow \quad \frac{s^2}{m} \sim \mathcal{O}\left(e^{+1/\alpha_s}\right), \quad (1.52)$$

this large logarithm completely **upends the standard perturbative power counting** in α_s .

The NLO cross section σ_{tot}^{qqg} containing one soft gluon bremsstrahlung is now **of the same order** as the LO elastic process, σ_{tot}^{qq} . And **two sequential emissions** of appropriately soft bremsstrahlung will **also be of the same order** as the LO process – and so on, for any number of soft gluon emissions. The limit (1.52) describes a **cascade of small- x_F gluons**, in which the large logarithms must be **resummed to all orders**. This results in a massive increase in the gluon density and in the abundance of particle production at high energies (synonymous with small x). The summation of $n = 0, 1, \dots, \infty$ gluons essentially **exponentiates** the one-loop kernel:

$$\begin{aligned} N_{tot}^g &\sim \sum_{n=0}^{\infty} \left(\alpha_s \times \ln \frac{s}{m^2} \times (\text{const}) \right)^n \\ &\sim \exp \left[\alpha_s \times \ln \frac{s}{m^2} \times (\text{const}) \right] \\ &\sim \left(\frac{s}{m^2} \right)^{\alpha_s \times (\text{const})}. \end{aligned}$$

This resummation process, in which the cross section at high energies grows as a power law in the energy, is sometimes referred to as **Reggeization**. The

1.2. Radiative Corrections: Soft QCD Bremsstrahlung

differential equation which expresses that leading-logarithmic resummation of soft gluon emission is known as the BFKL equation (Balitsky-Fadin-Kuraev-Lipatov), and its prediction of rapidly growing gluon densities in hadronic systems drives high-energy QCD toward the limit of nonlinear, high-density physics. If high-energy QCD induces a high density of gluons, then **nonlinear multiple scattering at all orders** will become important to characterize the high-energy asymptotic behavior of the theory. The physics of **coherent multiple scattering on a dense QCD system** is the essence of this high-energy limit, resulting in the landmark prediction of **gluon saturation**.

APPENDIX A

Background and Conventions

A.1 Review: Basics of QCD

Group Structure of $SU(3)$

Quantum Chromodynamics is the gauge theory of $SU(3)$ color symmetry. The gauge group $SU(3)$ consists of the group of **special, unitary, 3×3 matrices** which perform the color rotations among the 3 quark colors. The term “special” indicates that the matrices have **unit determinant**, which is the condition that excludes the unit matrix (“QCD photon”).

The 8 generators of $SU(3)$ in QCD are written

$$t^a = \frac{1}{2}\lambda^a \quad (\text{A.1})$$

where λ^a are the [Gell-Mann matrices](#)

$$\begin{aligned} \lambda^1 &= \begin{bmatrix} & 1 & \\ 1 & & \\ & & \end{bmatrix} & \lambda^2 &= \begin{bmatrix} & -i & \\ i & & \\ & & \end{bmatrix} & \lambda^3 &= \begin{bmatrix} 1 & & \\ & -1 & \\ & & \end{bmatrix} \\ \lambda^4 &= \begin{bmatrix} & & 1 \\ & & \\ 1 & & \end{bmatrix} & \lambda^5 &= \begin{bmatrix} & & -i \\ & & \\ i & & \end{bmatrix} & \lambda^6 &= \begin{bmatrix} & & \\ & & 1 \\ & 1 & \end{bmatrix} \\ \lambda^7 &= \begin{bmatrix} & & \\ & & -i \\ i & & \end{bmatrix} & \lambda^8 &= \frac{1}{\sqrt{3}} \begin{bmatrix} 1 & & \\ & 1 & \\ & & -2 \end{bmatrix} . \end{aligned} \quad (\text{A.2})$$

In this [fundamental representation](#) of $SU(3)$, the Gell-Mann matrices are these explicit 3×3 matrices, with the particular components t^3, t^8 being diagonal.

The essential property of $SU(3)$ is the Lie algebra of its generators, which can be expressed through the commutator relation

$$[t^a, t^b] = if^{abc} t^c, \quad (\text{A.3})$$

A. Background and Conventions

where f^{abc} are the totally antisymmetric structure constants

$$\begin{array}{c|cccccccc}
 f^{abc} & 1 & \frac{1}{2} & -\frac{1}{2} & \frac{1}{2} & \frac{1}{2} & \frac{1}{2} & -\frac{1}{2} & \frac{\sqrt{3}}{2} & \frac{\sqrt{3}}{2} \\
 \hline
 \text{a} & 1 & 1 & 1 & 2 & 2 & 3 & 3 & 4 & 6 \\
 \text{b} & 2 & 4 & 5 & 4 & 5 & 4 & 6 & 5 & 7 \\
 \text{c} & 3 & 7 & 6 & 6 & 7 & 5 & 7 & 8 & 8
 \end{array} \tag{A.4}$$

with $f^{abc} = -f^{bac} = -f^{acb}$ and all other components of f^{abc} equal to zero. The generators also satisfy a trace-orthogonality relation,

$$\text{tr}[\mathbf{1}] = N_c, \tag{A.5a}$$

$$\text{tr}[t^a] = 0, \tag{A.5b}$$

$$\text{tr}[t^a t^b] = \frac{1}{2} \delta^{ab}, \tag{A.5c}$$

and the sum of the squares of the generators is a special invariant of the group called the [quadratic Casimir element](#),

$$t^a t^a = C_F \mathbf{1} \equiv \left(\frac{N_c^2 - 1}{2N_c} \right) \mathbf{1}. \tag{A.6}$$

For real QCD with the gauge group $SU(3)$, the group constants are $N_c = 3$ and $C_F = 4/3$.

The structure constants f^{abc} themselves provide the 8-dimensional [adjoint representation](#) of $SU(3)$ (which we denote here in capital letters),

$$(T^a)_{bc} \equiv -i f^{abc}, \tag{A.7}$$

which satisfies the Lie (commutator) algebra [\(A.3\)](#)

$$[T^a, T^b] = i f^{abc} T^c \tag{A.8}$$

through the use of the Jacobi identity

$$[T^a, [T^b, T^c]] + [T^b, [T^c, T^a]] + [T^c, [T^a, T^b]] = 0. \tag{A.9}$$

Just as the 3×3 fundamental representation of $SU(3)$ describes the color states of the quarks and how they transform, the 8×8 adjoint representation describes the color states and interactions of the **gluons**. In a general $SU(N_c)$ gauge group, the fundamental representation has dimension N_c and the adjoint representation has dimension $(N_c^2 - 1)$.

The t'Hooft Large- N_c Limit

While for true QCD the number of quark colors is 3, the general gauge structure of QCD is only minimally modified for the case of arbitrary number of quark colors N_c . We have already benefited from the comparison of QCD ($N_c = 3$) with the Pauli matrices of $N_c = 2$. In fact, the algebra of the general gauge

group $SU(N_c)$ becomes significantly **simpler** with clever usage of the number of colors N_c . One particularly powerful usage is the **t’Hooft large- N_c limit**

$$\alpha_s \rightarrow 0, \quad (\text{A.10a})$$

$$N_c \rightarrow \infty, \quad (\text{A.10b})$$

$$\alpha_s N_c = \text{const} \ll 1. \quad (\text{A.10c})$$

In this limit, the “S” of $SU(N_c)$ essentially becomes irrelevant (reducing $SU(N_c)$ to $U(N_c)$), since the one omitted generator is negligible compared to the $N_c^2 - 1 \approx N_c^2$ generators retained as $N_c \rightarrow \infty$. This can be clearly seen in the form of the Fierz identity for $SU(N_c)$

$$(t^a)^i_j (t^a)^k_\ell = \frac{1}{2} \delta^i_\ell \delta^k_j - \frac{1}{2N_c} \delta^i_j \delta^k_\ell \stackrel{N_c \gg 1}{\approx} \frac{1}{2} \delta^i_\ell \delta^k_j, \quad (\text{A.11})$$

where the subtraction term enforcing $(t^a)^i_i = 0$ drops out.

In the large- N_c limit, the number of gluons $N_c^2 - 1$ far exceeds the number of quarks N_c , so this limit **simplifies QCD to effectively contain only gluons**. For gluon-dominated phenomena like small- x gluon saturation, this approximation is an especially powerful simplification. The simplified Fierz identity (A.11) allows the adjoint color flow of gluons to be replaced with an equivalent fundamental color flow, as if the gluon were being replaced by a quark-antiquark pair¹. Moreover, the Feynman diagrams which dominate the large- N_c limit are always **planar**, meaning that (in a graph theory sense), all the vertices and propagators can be laid out flat on a plane, without any lines needing to cross “underneath” each other to construct the diagram. This can lead to a tremendous simplification of the color structure and associated operators for high-energy scattering in QCD, making the large- N_c limit highly advantageous in QCD. As an approximation to QCD, corrections to the large- N_c limit in real QCD often occurs at $\mathcal{O}(1/N_c^2)$ for physical observables. One would accordingly expect that the large- N_c limit is accurate at the level of $1/9 \sim 10\%$; however, for many observables, the large- N_c limit works even better in practice than this naive estimate.

A.2 The QCD Lagrangian

Gauge Symmetry

Under a local $SU(N_c)$ gauge transformation, the quark and gluon fields transform as

$$\psi' = e^{i\phi^a t^a} \psi, \quad (\text{A.12a})$$

$$A^{\mu a'} = A^{\mu a} + \frac{1}{g} (\partial^\mu \phi^a) + f^{abc} A^{\mu b} \phi^c. \quad (\text{A.12b})$$

¹Caution: this statement applies only to the color representation, not to any other quantum numbers such as spin.

A. Background and Conventions

Interestingly, for a non-Abelian gauge theory like QCD, both a shift of $A^{\mu a}$ by a scalar-polarized mode ($\partial^\mu \phi^a$) and a color rotation of $A^{\mu a}$ correspond to a gauge transformation.

The derivative operator which compensates for any local change of gauge is the **gauge-covariant derivative**

$$D_\mu \equiv \partial_\mu - ig A_\mu^a t^a, \quad (\text{A.13a})$$

$$(D_\mu \psi)' = e^{i\phi^a t^a} (D_\mu \psi) \quad (\text{A.13b})$$

From the covariant derivative, we can similarly construct a properly gauge-covariant field-strength tensor $F_{\mu\nu}^a$ using the commutator:

$$[D_\mu, D_\nu] = [\partial_\mu - ig A_\mu^a t^a, \partial_\nu - ig A_\nu^b t^b] \equiv -ig F_{\mu\nu}^c t^c, \quad (\text{A.14})$$

where

$$F_{\mu\nu}^c \equiv \partial_\mu A_\nu^c - \partial_\nu A_\mu^c + gf^{abc} A_\mu^a A_\nu^b. \quad (\text{A.15})$$

Note that, in an Abelian theory like QED, the covariant derivative and field-strength tensor are rather trivial:

$$D_\mu \stackrel{QED}{\equiv} \partial_\mu + ie A_\mu, \quad (\text{A.16a})$$

$$[D_\mu, D_\nu] = ie(\partial_\mu A_\nu - \partial_\nu A_\mu) = ie F_{\mu\nu}. \quad (\text{A.16b})$$

But in QCD, the field-strength tensor (A.15) contains more than just the free kinetic part, linear in A^μ , which occurs in QED. This is because, unlike in QED, now the free part ($\partial_\mu A_\nu^a - \partial_\nu A_\mu^a$) is **not gauge invariant** (or even gauge covariant). Instead, the ‘‘chromo-electric’’ and ‘‘chromo-magnetic’’ fields are themselves not separately gauge invariant, since they can be changed by a color rotation. Note that, while field-strength tensor $F_{\mu\nu}^a$ for a given color a is not gauge invariant, its **square** (summed over colors) is:

$$F_{\mu\nu}^a F^{\mu\nu a} = F_{\mu\nu}^a F^{\mu\nu a}. \quad (\text{A.17})$$

Lagrangian and Feynman Rules

From the appropriate $SU(N_c)$ -covariant ingredients, the quark field ψ , the covariant derivative D_μ , and the field-strength tensor $F_{\mu\nu}^a$, we can immediately write down the QCD Lagrangian,

$$\begin{aligned} \mathcal{L}_{QCD} &= \bar{\psi}(i\not{D} - m)\psi - \frac{1}{4}F_{\mu\nu}^a F^{\mu\nu a} \\ &= \bar{\psi}(i\not{\partial} - m)\psi - \frac{1}{4}(\partial_\mu A_\nu^a - \partial_\nu A_\mu^a)(\partial^\mu A^{\nu a} - \partial^\nu A^{\mu a}) \\ &\quad + g\bar{\psi}\gamma_\mu t^a \psi A^{\mu a} - gf^{abc} A_\mu^b A_\nu^c (\partial^\mu A^{\nu a}) \end{aligned}$$

A.2. The QCD Lagrangian

Figure A.1: Feynman rules for the interaction vertices in QCD. These ingredients give the contributions to any scattering amplitude $i\mathcal{M}$.

$$-\frac{1}{4}g^2 f^{abc} f^{ab'c'} A_\mu^b A_\nu^c A^{\mu b'} A^{\nu c'} . \quad (\text{A.18})$$

From the Lagrangian (A.18), we can readily compute the Feynman rules shown in Fig. A.1. While the quark/gluon vertex is highly similar to the equivalent QED electron/photon vertex up to a color factor, the 3-gluon and 4-gluon vertices are entirely new. These arise from the non-Abelian corrections to the pure glue part $-\frac{1}{4}F_{\mu\nu}^a F^{\mu\nu a}$. Note that the 3-gluon vertex is momentum dependent, arising from its derivative coupling, while the 4-gluon vertex is momentum independent. Both are proportional to the non-Abelian structure constants f^{abc} .

These new gluonic self-interactions have many profound consequences for QCD, but none is more important than their role in the QCD vacuum polarization shown in Fig. A.2. Because of the non-Abelian nature of QCD, not only fermions (quarks) enter the virtual loops contributing to the vacuum polarization; gluon loops enter as well. And the gluon loops **compete** with the quark loops: while the quarks produce a positive contribution to the beta function (as with electrons in QED), the gluons make a **negative** contribution to the beta function:

$$\beta_g = \frac{1}{3} \frac{g^3}{(4\pi)^2} (2N_f - 11N_c) , \quad (\text{A.19})$$

where N_f is the number of quark flavors entering the loop and N_c is the number of quark colors. For QCD, the **gluons win**, resulting in a beta function which is **negative**.

This negative beta function is the hallmark of QCD, resulting in a running coupling $\alpha_s(Q^2)$ which **decreases** with increasing momentum scale Q^2 – the **opposite** of an Abelian theory like QED. This negative beta function results in both the phenomenon of **asymptotic freedom** ($\alpha_s(Q^2) \rightarrow 0$ as $Q^2 \rightarrow \infty$) as well as **confinement** ($\alpha_s(Q^2) \rightarrow \infty$ as $Q^2 \rightarrow 0$). Unlike QED, which possesses its Landau pole in the UV limit $Q^2 \rightarrow \infty$, the negative beta function of QCD places its Landau pole in the IR regime $Q^2 \rightarrow 0$. This signifies the onset of

A. Background and Conventions

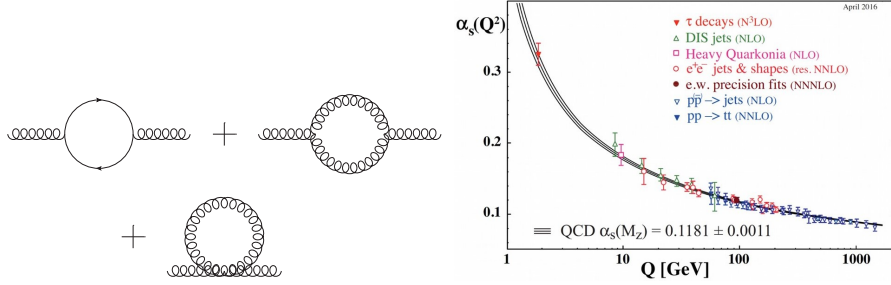


Figure A.2: Effect of the non-Abelian vertices on the QCD running coupling.

the confinement phase transition at nonperturbative coupling in QCD in the IR, in contrast to the electroweak phase transition of QED in the UV. The other profound implication of asymptotic freedom is that **QCD is a valid, self-consistent theory up to *infinitely high* momentum scales**. What asymptotic freedom buys us is **UV completeness**: an essential property of any candidate fundamental theory of nature, which is elegantly and automatically satisfied by non-Abelian gauge theories like QCD.

A.3 Other Notation and Conventions

Light-Front Components

A four-vector p^μ may be expressed in terms of **light-front coordinates**, which are linear combinations of the timelike component and one spacelike component (usually chosen to be the z -component). There are two light-front components, p^+ and p^- , defined by

$$p^\pm \equiv \frac{1}{\sqrt{2}}(p^0 \pm p^3). \quad (\text{A.20})$$

In terms of light-front components, four-vector products take the form

$$p \cdot q = p^+ q^- + p^- q^+ - \vec{p}_\perp \cdot \vec{q}_\perp, \quad (\text{A.21})$$

and for an on-shell particle with given p^+ and \vec{p}_\perp , the on-shell condition fixes the other light-front component to be

$$\begin{aligned} p^2 &= 2p^+ p^- - \vec{p}_\perp^2 = m^2 \\ \therefore p^- &= \frac{\vec{p}_\perp^2 + m^2}{2p^+}. \end{aligned} \quad (\text{A.22})$$

A particle moving at high energy along the $+z$ axis with $p^0 \approx p^3 \approx E$ therefore has $p^+ \approx \sqrt{2}E \rightarrow \infty$ and $p^- \approx (\vec{p}_\perp^2 + m^2)/(2\sqrt{2}E) \rightarrow 0$. The reverse is true for a particle moving along the $-z$ axis.

A.3. Other Notation and Conventions

We will denote vectors written in terms of their light-front components using square brackets, and we will often emphasize which component is which by a superscript. For instance, the momentum of an on-shell particle of mass m moving along the z -axis may be written

$$\begin{aligned} p^\mu &= [p^+, p^-, \vec{p}_\perp]^\mu \\ &= \left[p^+, \frac{p_\perp^2 + m^2}{2p^+}, \vec{p}_\perp \right]^\mu \\ &\rightarrow [p^+, 0^-, \vec{p}_\perp]^\mu, \end{aligned} \tag{A.23}$$

where the last line follows in the ultrarelativistic limit $p^+ \rightarrow \infty$. Equivalently, we may use the on-shell condition to solve for p^+ in terms of p^- , which is convenient for describing a particle moving along the $-z$ axis at high energy:

$$\begin{aligned} p^\mu &= [p^+, p^-, \vec{p}_\perp]^\mu \\ &= \left[\frac{p_\perp^2 + m^2}{2p^-}, p^-, \vec{p}_\perp \right]^\mu \\ &\rightarrow [0^+, p^-, \vec{p}_\perp]^\mu, \end{aligned} \tag{A.24}$$

where the last line follows in the limit $p^- \rightarrow \infty$.